

# A Hosford-based orthotropic plasticity model in LS-DYNA

Filipe Andrade<sup>1</sup>, Thomas Borrvall<sup>2</sup>, Paul DuBois<sup>3</sup>, Markus Feucht<sup>4</sup>

<sup>1</sup>DYNAmore GmbH, Stuttgart, Germany

<sup>2</sup>DYNAmore Nordic AB, Linköping, Sweden

<sup>3</sup>Consultant, Detroit MI, USA

<sup>4</sup>Daimler AG, Sindelfingen, Germany

## 1 Introduction

In this contribution, we present a new orthotropic plasticity model available in LS-DYNA. Over the last decades, several orthotropic material models have been proposed in the literature where many of them have been implemented in LS-DYNA. Among these models, the model proposed by Barlat and Lian in 1989 [1], available in LS-DYNA in \*MAT\_036 [2], is a popular choice, especially in forming simulations. This model allows the user to define up to three R values (Lankford parameters) related to three material directions, namely 0°, 45° and 90° with respect to the rolling direction. Some years ago, the original orthotropic formulation by Barlat and Lian, available under \*MAT\_036 in LS-DYNA, was extended in such manner that the yield stress can depend on the different material directions. From a user point of view, this meant that up to five flow curves could be defined. Furthermore, up to five R values could also be used where these could be either constant or a function of the plastic strain. In \*MAT\_036, the extended model is activated by setting the flag HR to 7. However, the extended formulation incorporates the orthotropy in the yield stress as well. The consequence is that these two effects (orthotropy in the effective stress and also in the yield stress) concur against each other. For many materials, especially mild sheet steels, this aspect has often no major influence on the results. However, certain materials do exhibit quite dissimilar R values in the different material directions meanwhile the yield strength is very similar. This is, for instance, the case of many aluminum alloys. In such cases, the extended formulation available through HR=7 in \*MAT\_036 (or HOSF=0 in \*MAT\_036E) might lead to concave yield surfaces which, in turn, might lead to numerical instabilities. Therefore, a new option, issued through the flag HOSF, has been implemented in LS-DYNA in \*MAT\_036E. If HOSF is set to 1, a “Hosford-based” effective stress is used in yield function. This modification tends to alleviate the numerical instabilities observed in the model where the “Barlat-based” effective stress was used whenever the R values were very dissimilar. In a certain sense, the modification can be seen as a new plasticity model because in the new formulation the yield condition is not formulated using any information related to the R values but merely from the flow curves in the different directions. The R values are instead only used in the plastic flow rule. In this paper, we will show the advantages of such formulation as well as the results of the calibration of the material parameters for an aluminum sheet material. The results show that the simulation with the new material model can reproduce the strain fields captured in experiments through DIC very accurately.

## 2 Material modeling

In this section, we review some concepts regarding the modeling of orthotropic materials and present the new modification using a Hosford-based effective stress.

### 2.1 The Lankford parameter

The Lankford parameter [3], also commonly called “R value”, is a parameter used to better characterize the deformation behavior of thin materials. Its definition slightly varies in the literature where usually total strains are used but sometimes strain increments are also considered. Nevertheless, one can basically assume that it relates the strains (or strain increments) between the second and third directions where the first direction is the direction of the applied load. In this paper, we consider

$$R = \frac{\epsilon_2^p}{\epsilon_3^p} \quad (1)$$

It is important to remark that Eq. (1) is only adopted for a uniaxial stress state (e.g., in a tensile test up to the necking) provided that the load is applied in direction “1”. In other words, the R value relates the strains of the two directions in which no load is applied. In this respect, the R value should not be confused with the Poisson’s ratio,  $\nu$ , which relates one of the transversal strains with the strain in the direction of the applied load.

From a practical point of view, the R value can be quite useful. If known, the R value allows a quick assessment if a certain material is adequate for deep drawing operations, for instance. This is possible because the second and third strains can be respectively interpreted as indicators for the amount of necking and thinning of the material when subjected to plastic straining under a uniaxial condition (see schematic representation in Fig. 1). For example, if  $\varepsilon_2 = \varepsilon_3$ , this means that the amount of necking is of the same magnitude than the amount of thinning which, in turn, leads to a value of  $R=1$ . If  $\varepsilon_2 < \varepsilon_3$ , the amount of thinning is larger than the amount of necking and the R value assumes a value of  $R<1$ . Finally, for  $\varepsilon_2 > \varepsilon_3$ , more necking takes place if compared to the thinning, leading to  $R>1$ .

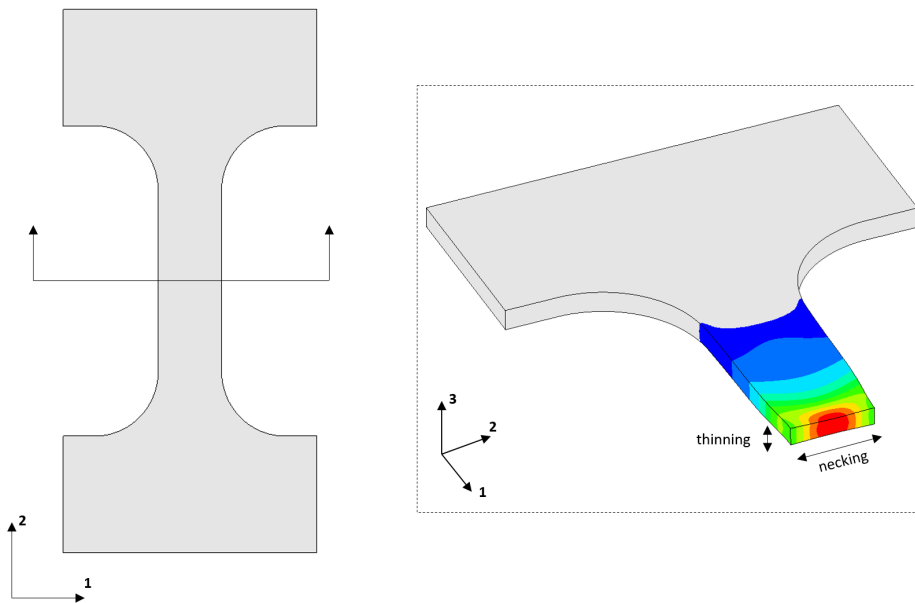


Fig.1: Necking and thinning of a tensile test.

In practice, the R value is measured in different material directions. Typically, the 0°, 45° and 90° orientations with respect to the rolling direction are tested. Usually, the R values obtained are then different from one another, although this depends on the material itself. For instance, deep draw sheet steels typically exhibit high R values ( $R>1$ ) and are, to some extent, similar to each other. In the case of aluminum extrusions, the R values can be quite dissimilar where one direction has a value much larger than 1.0 and the other direction has a value much smaller than 1.0.

As a matter of fact, the R value is very useful in practical terms due to its easiness of interpretation. Furthermore, the R value is also rather easy to measure experimentally. Consequently, it is also generally desired the use of the R value directly in the definition of the material model. In the next sections, we will discuss how measured R values can be used when defining a material card for \*MAT\_036 and \*MAT\_036E and the consequences of its use in the different constitutive formulations.

## 2.2 Original orthotropic model by Barlat and Lian (1989)

This model was proposed by Barlat and Lian in 1989 [1] and it is implemented in LS-DYNA under \*MAT\_036 (or \*MAT\_3-PARAMETER\_BARLAT), see LS-DYNA Keyword User’s Manual Vol. 2 [2]. The yield function is defined as

$$\Phi(\sigma) = \frac{1}{2} (a|K_1 + K_2|^m + a|K_1 - K_2|^m + c|2K_2|^m) - \sigma_y^m = 0 \quad (2)$$

where

$$K = \frac{\sigma_x + h \sigma_y}{2}, \quad K_2 = \sqrt{\left(\frac{\sigma_x - h \sigma_y}{2}\right)^2 + p^2 \sigma_{xy}^2} \quad (3)$$

As can be seen in Equations (2) and (3), this model does not explicitly have the R values in the formulation of the yield function. Nevertheless, Barlat and Lian have shown that it is possible to correlate the material parameters a, c, h and p to the R values through

$$a = 2 - 2\sqrt{\left(\frac{R_0}{1+R_0}\right)\left(\frac{R_{90}}{1+R_{90}}\right)}, \quad c = 2 - a, \quad h = \sqrt{\left(\frac{R_0}{1+R_0}\right)\left(\frac{1+R_{90}}{R_{90}}\right)} \quad (4)$$

The parameter “p” can be iteratively determined from

$$R_{45} = \frac{2m\sigma_y^m}{\left(\frac{\partial\Phi}{\partial x} + \frac{\partial\Phi}{\partial y}\right)\sigma_{45}} \quad (5)$$

In LS-DYNA, the user can either input the parameters a-c-h-p or, instead, input the R values directly. In this case, LS-DYNA will internally compute the parameters a, c, h and p that match the R values specified by the user. The flow rule, which in essence determines how the material behaves under the plastic regime, is associated, i.e.,

$$\dot{\epsilon}^p = \begin{bmatrix} \dot{\epsilon}_{11}^p & \dot{\epsilon}_{12}^p & \dot{\epsilon}_{13}^p \\ \dot{\epsilon}_{21}^p & \dot{\epsilon}_{22}^p & \dot{\epsilon}_{23}^p \\ \dot{\epsilon}_{31}^p & \dot{\epsilon}_{32}^p & \dot{\epsilon}_{33}^p \end{bmatrix} = \dot{\gamma} \frac{\partial\Phi}{\partial\sigma} \quad (6)$$

It is important to emphasize that in this model the R values have a direct influence on the yield surface. For R values which are more or less similar, the difference between the yield stress in 0° and 90° is rather small, matching typical values observed in experiments. If the R values differ significantly from one another (e.g. in the case of aluminum extrusions), the difference between the yield stress in 0° and 90° is quite substantial. However, this behavior is not usually observed in physical tests of typical sheet steel and aluminum alloys. The effect of different combinations of R values when used in conjunction with the constitutive model by Barlat and Lian from 1989 can be seen in Fig. 2 where \*MAT\_036 was used with the option HR=3 (i.e., three R values and one single hardening curve for the 0° direction). The associated yield loci are depicted in Fig. 3.

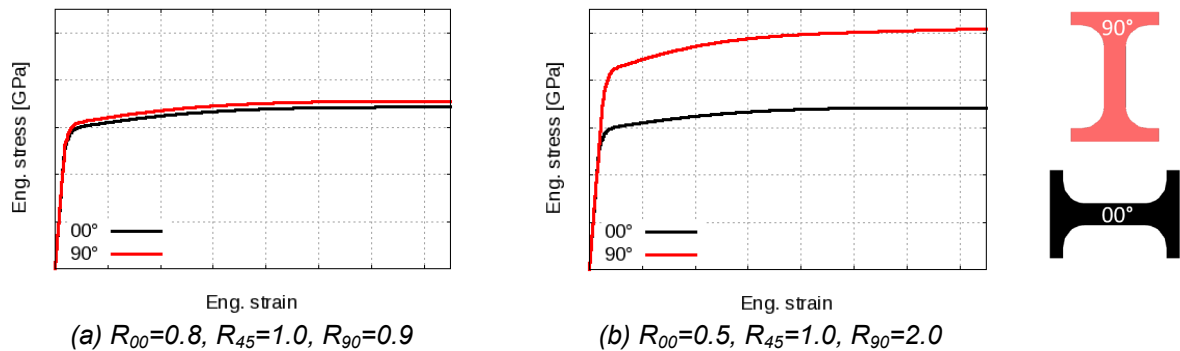


Fig.2: Engineering stress strain curves of the simulation of a tensile test using \*MAT\_036 and HR=3.

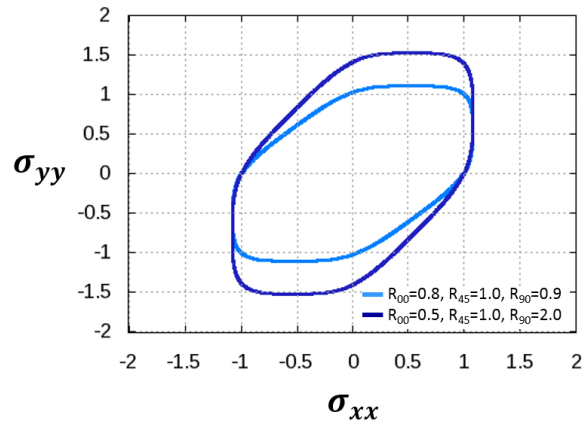


Fig.3: Yield locus for different combinations of R values with the Barlat and Lian model ( $m=8$ ,  $\sigma_{xy}=0.0$ )

### 2.3 Extension of \*MAT\_036 through the flag HR=7

The implementation of \*MAT\_036 was extended in order to take into account several hardening curves in the different directions [2]. The new yield function, which is based on the Barlat and Lian model, is written as

$$\Phi(\boldsymbol{\sigma}) = \frac{1}{2} (a|K_1 + K_2|^m + a|K_1 - K_2|^m + c|2K_2|^m) - \sigma_y^m (\sigma_y^0, \sigma_y^{45}, \sigma_y^{90}, \sigma_y^s, \sigma_y^b) = 0 \quad (7)$$

where now the yield stress is itself a function of the hardening curves in the 0°, 45° and 90° directions as well as the hardening curves under shear and equibiaxial tension. It is worth noting that the shear and equibiaxial hardening curves are not mandatory [2]. The enhanced model can be activated in \*MAT\_036 by setting HR to 7 or directly in \*MAT\_036E (both inputs are equivalent).

Due to the consideration of hardening curves in the different directions, the extended model is able to correct the overestimation of the yield stress in certain directions in case of very dissimilar R values. This can be seen in Fig. 4 where the same parameters from Section 2.2. were used with difference that now three hardening curves were also given in the input. In this example, the hardening curve in the 90° is example almost identical to the one in the 0° direction, leading to basically the same engineering stress strain curve in both directions. The main difference lies on the local strain field of the tensile sample which is different due to the different R values.

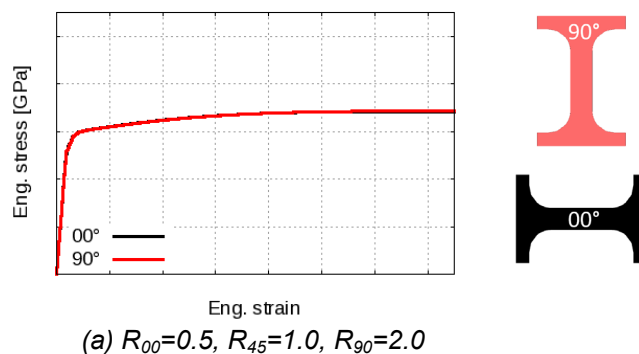


Fig.4: Engineering stress strain curve of the simulation of a tensile test using \*MAT\_036 and HR=7 (with three hardening curves in the 0°, 45° and 90° directions).

The local strain field in such a tensile test simulation matches the R values defined by the user in the input. This is achieved by modifying the flow rule such that

$$\dot{\boldsymbol{\varepsilon}}^p = \begin{bmatrix} \dot{\varepsilon}_{11}^p & \dot{\varepsilon}_{12}^p & \dot{\varepsilon}_{13}^p \\ \dot{\varepsilon}_{21}^p & \dot{\varepsilon}_{22}^p & \dot{\varepsilon}_{23}^p \\ \dot{\varepsilon}_{31}^p & \dot{\varepsilon}_{32}^p & \dot{\varepsilon}_{33}^p \end{bmatrix} = \dot{\gamma} \left( \frac{\partial \Phi}{\partial \boldsymbol{\sigma}} + \Delta \mathbf{N} \right) \quad (8)$$

where  $\Delta \mathbf{N}$  is the smallest increment necessary to match the experimental R values. This causes this model to be non-associated.

Although the extended model can effectively correct any overestimation of the yield stress in different directions, it still considers the a-c-h-p parameters in the yield function, similar to the original formulation by Barlat and Lian. As mentioned in Section 2.2, these parameters can be related to the R values which, in turn, also influence the yield surface. As a matter of fact, the a-c-h-p parameters as well as the different hardening curves have a direct influence on the yielding point. This means that both these effects concur with each other.

The original idea behind the extended formulation was to not deviate too much from the original model by Barlat and Lian [1]. In fact, when the R values are more or less well behaved (a typical situation for many sheet materials), this formulation does not cause any numerical difficulties. However, for very dissimilar R values, the concurring effect of the a-c-h-p parameters and the hardening curves in the different directions may (but does not necessarily) lead to a concave yield surface. This can be seen in Fig. 5 where different combinations of R values are shown as an example of this behavior. Concave yield surfaces can be critical because they do not guarantee plastic dissipation a priori. In other words, such yield surfaces may introduce energy in the system. However, plastic behavior is actually dissipative. Nonetheless, convergence of the material model may be achieved but instabilities can still occur depending on the loading path. For example, Fig. 6 shows one case where oscillations were observed in the simulation of a notched tensile test in the  $90^\circ$  direction. However, the same oscillations did not occur in the  $0^\circ$  direction because, for that particular loading path, the yield surface is well behaved.

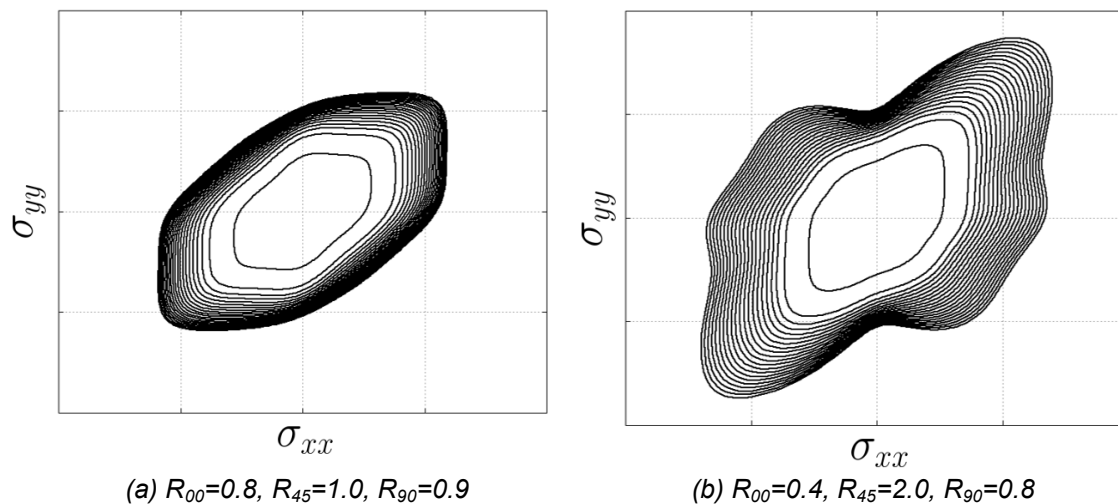


Fig. 5: Yield locus for different combinations of R values when using \*MAT\_036 and HR=7 (using three hardening curves). The different lines represent different levels of plastic strain.

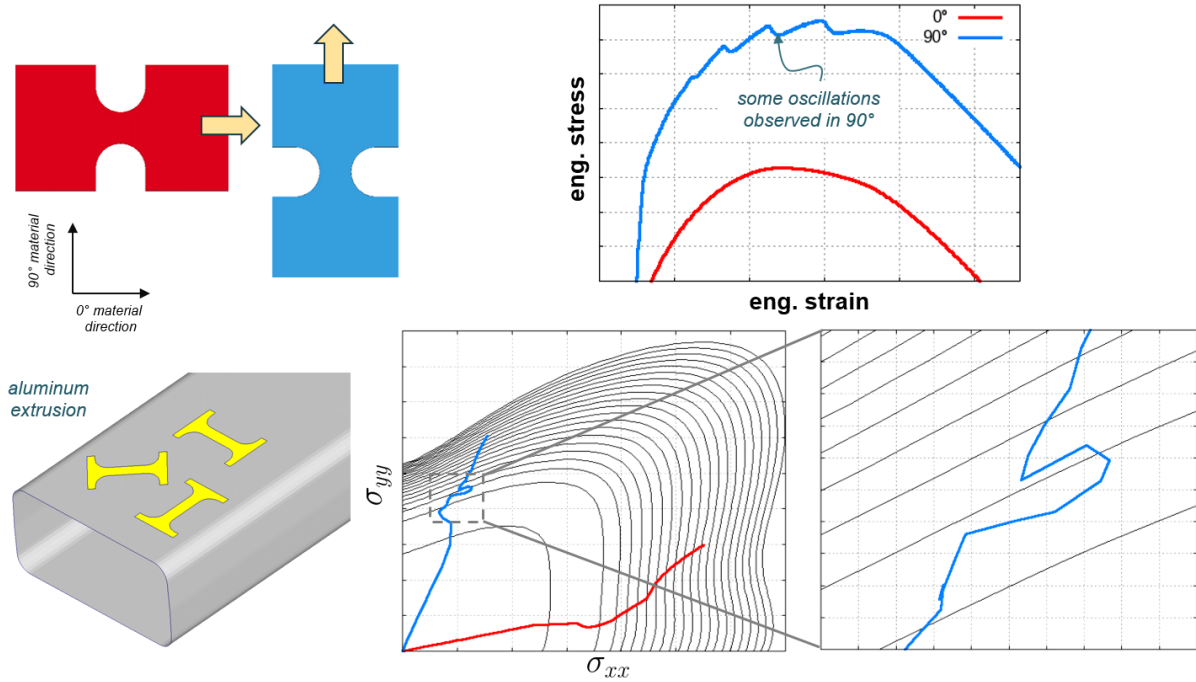


Fig.6: Oscillations observed in the simulation of a notched tensile test with \*MAT\_036 and HR=7 (three hardening curves,  $R_{00}=0.4$ ,  $R_{45}=2.0$ ,  $R_{90}=0.8$ )

#### 2.4 Proposed modification: A Hosford-based model (\*MAT\_036E with HOSF=1)

Due to the oscillations observed in certain cases when using the extended Barlat and Lian model (i.e., \*MAT\_036 with HR=7), a modification of the yield function is proposed in order to avoid concave yield surfaces. If the material and principal axes are coincident, the new yield function can be written as

$$\Phi(\boldsymbol{\sigma}) = \frac{1}{2} (|\sigma_1|^m + |\sigma_2|^m + |\sigma_1 - \sigma_2|^m) - \sigma_y^m(\sigma_y^0, \sigma_y^{45}, \sigma_y^{90}, \sigma_y^s, \sigma_y^b) = 0 \quad (9)$$

The main difference is that Eq. (7) contains the orthotropic parameters a-c-h-p in the yield function meanwhile the new yield function in Eq. (9) contains information about the anisotropy only in the hardening curves. The first part of the equation can be seen as an effective stress used in the yield criterion, i.e.,

$$\sigma_{eff} = \frac{1}{2} (|\sigma_1|^m + |\sigma_2|^m + |\sigma_1 - \sigma_2|^m) \quad (10)$$

In fact, an identical effective stress was proposed by Hosford [4] when he generalized the von Mises criterion. Therefore, one can say that the new model has a Hosford-based effective stress. The new model can be activated in LS-DYNA (version R11 or later) in \*MAT\_036E by setting the flag HOSF=1. If HOSF=0, then the model of Section 2.3 (Equation 7) is used. A summary of the differences between HOSF=0 and HOSF=1 is given in Table 1.

Identically to the model of Section 2.3, the (non-associated) flow rule is given by

$$\dot{\boldsymbol{\varepsilon}}^p = \begin{bmatrix} \dot{\varepsilon}_{11}^p & \dot{\varepsilon}_{12}^p & \dot{\varepsilon}_{13}^p \\ \dot{\varepsilon}_{21}^p & \dot{\varepsilon}_{22}^p & \dot{\varepsilon}_{23}^p \\ \dot{\varepsilon}_{31}^p & \dot{\varepsilon}_{32}^p & \dot{\varepsilon}_{33}^p \end{bmatrix} = \dot{\gamma} \left( \frac{\partial \Phi}{\partial \boldsymbol{\sigma}} + \Delta \mathbf{N} \right) \quad (11)$$

	Effective Stress	Yield function	Influence of the R values
<b>HOSF = 0</b>	Barlat-Based	Eq. (7)	On yield function and flow rule
<b>HOSF = 1</b>	Hosford-Based	Eq. (9)	On the flow rule only

Table 1: Effect of the flag HOSF in \*MAT\_036E

In Eq. (11),  $\Delta N$  is, again, the smallest increment necessary to match the experimental R values.

To some extent, the modification can be seen as a new plasticity model because in the new formulation the yield condition is not formulated using any information related to the R values but merely from the flow curves in the different directions. The R values are instead only used in the plastic flow rule, leading to a non-associated plasticity model. This eliminates the concurring mechanisms coming from orthotropic plastic yielding and orthotropic plastic flow, providing a more sound and stable plasticity model.

The Hosford-based model has then been adopted in the simulation of the notched test in the 90° direction for which oscillations were observed when running the simulation with \*MAT\_036 with HR=7 (i.e., \*MAT\_036E with HOSF=0). The results are shown in Figure 7. As can be seen in the diagrams, the yield surface with HOSF=1 is much more well behaved than the one with HOSF=0. Furthermore, the use of the formulation provided with HOSF=1 is able to significantly alleviate the observed oscillations.

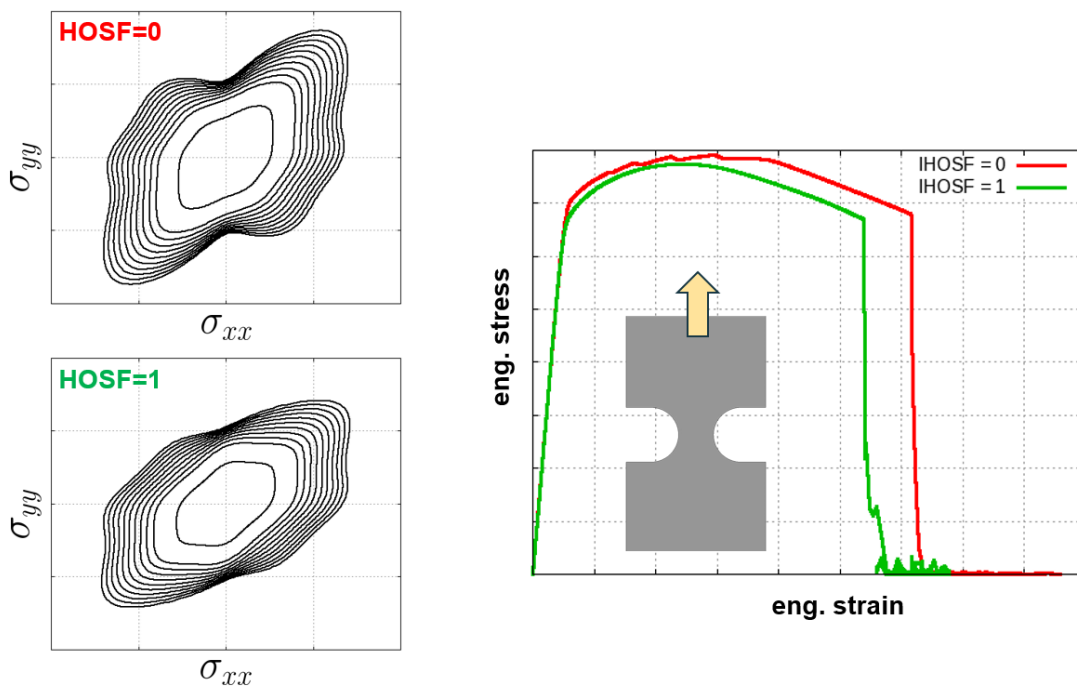


Fig.7: Comparison between HOSF=0 and HOSF=1 for  $R_{00}=0.4$ ,  $R_{45}=2.0$ ,  $R_{90}=0.8$ , simulation of a notched test in the 90° direction.

### 3 Numerical Simulation – Aluminum Sheet

In this section, we assess the ability of the new constitutive model to reproduce the experimental data of an aluminium sheet (thickness around 1.5mm) used in the automotive industry. The material was physically tested at the laboratories of DYNAmore, in Stuttgart, by Koch, Helbig and Ilg [5]. A digital image correlation system was used in order to measure the local strain fields. The mean R values measured in the three directions were  $R_{00}=0.7$ ,  $R_{45}=0.5$  and  $R_{90}=0.8$ . These values were directly used in the material card and were assumed to be constant throughout deformation. The material model used was \*MAT\_036E with the HOSF flag set to 1. Shell elements (ELFORM=16) were adopted in the calibration of the material card where three hardening curves were identified (see Fig. 6a). Shell thickness update was activated through \*CONTROL\_SHELL, ISTUPD=1. Fig. 6b shows the match between simulation and experimental engineering stress strain curves for the three directions.

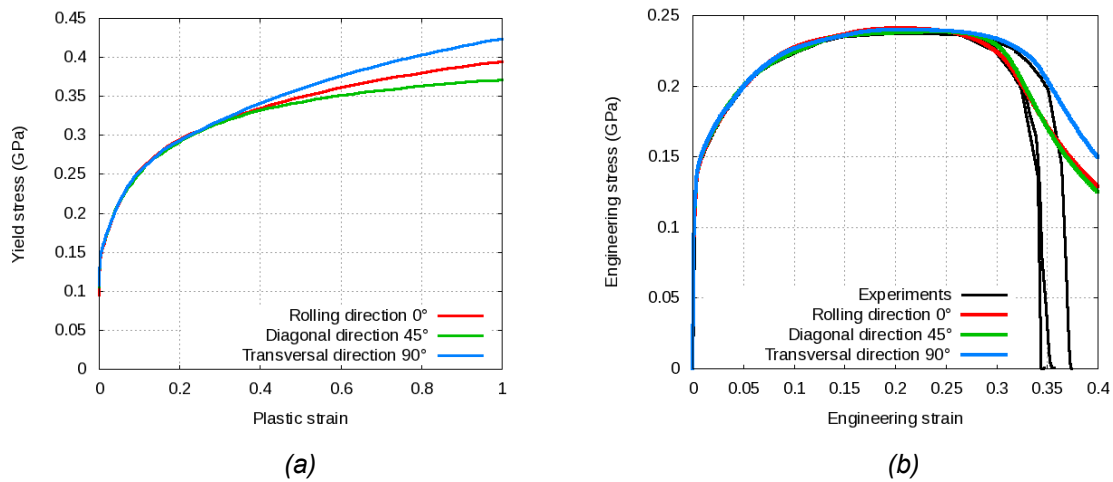


Fig.8: (a) Hardening curves calibrated for \*MAT\_036E with HOSF=1. (b) Experimental and simulation stress strain curves with \*MAT\_036E with HOSF=1

In Figures 9-11, the local strain fields from the simulations are compared with the strain fields optically measured and processed using digital image correlation. As can be seen in the figures, the simulation results agree very well with the experimental results. In the plots, a similar color scheme as the one available in LS-PrePost was adopted in order to facilitate the comparison. Furthermore, especial care was taken in using the same scale for the color legend. The point of evaluation was chosen based on the experimental record. Close to failure, the DIC software may lose resolution, resulting in “holes” in the picture of the local strain field. Therefore, a state as close as possible to failure was chosen for which the whole strain field could still be evaluated without loss of resolution. The selected evaluation points are depicted in the engineering stress strain curves next to the contour plots.

It is worth mentioning that, although the engineering strain at failure for the three different directions is more or less similar (see Fig. 8b), the local (true) strain at failure does exhibit some variation. In the 0°, the maximum value was around  $\epsilon_p=0.7$  meanwhile in the 45° direction a value of around  $\epsilon_p=0.615$  was observed. The use of the new material model was able to capture that orientation dependence very accurately. An isotropic material model (e.g. \*MAT\_024) would be able to capture the engineering strain at failure, but only one of the different local strain fields would be reproduced. Therefore, if accuracy of local strains is an issue, the new material model can be quite useful in describing the material behavior.

It should also be noted that the use of HOSF=0 delivers almost identical results for these tensile specimens. However, when looking closely to the yield surface for HOSF=0, one can see that a slight concavity is present. Convexity can be achieved by using HOSF=1 (see Fig. 12). Therefore, when using the present material parameters in the simulation of other geometries whose loading paths might be more nonlinear than the ones of a simple tensile test, HOSF=1 would avoid any numerical difficulties that may arise.



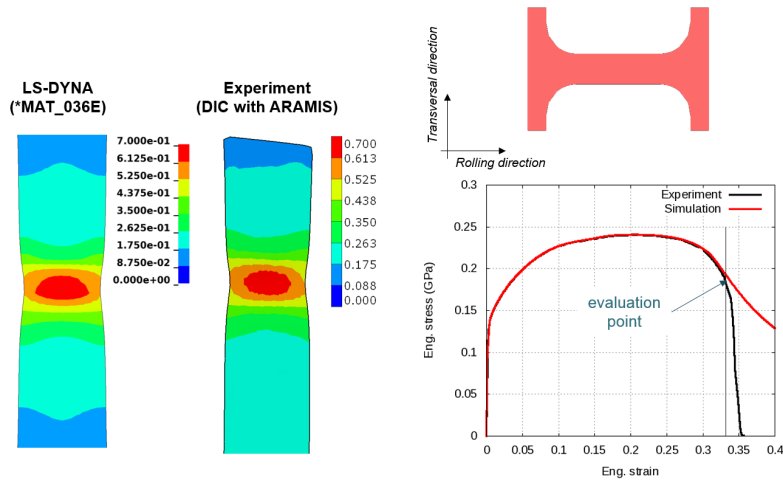


Fig.9: Comparison between experiment and simulation for the 0° direction

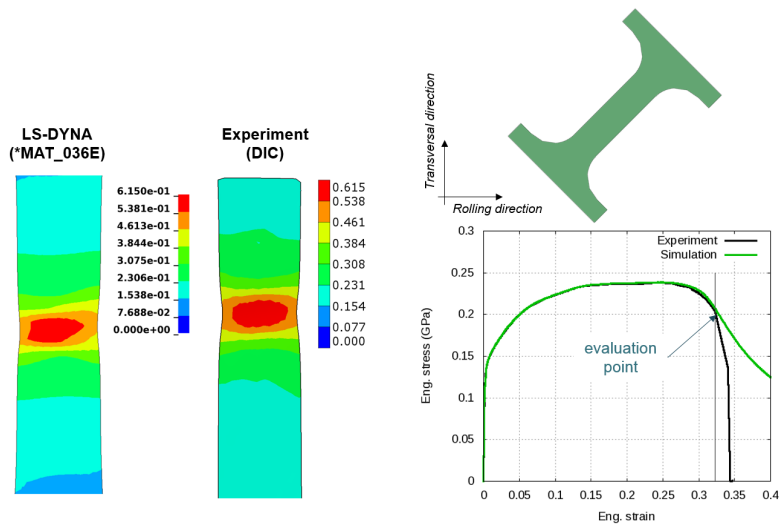


Fig.10: Comparison between experiment and simulation for the 45° direction

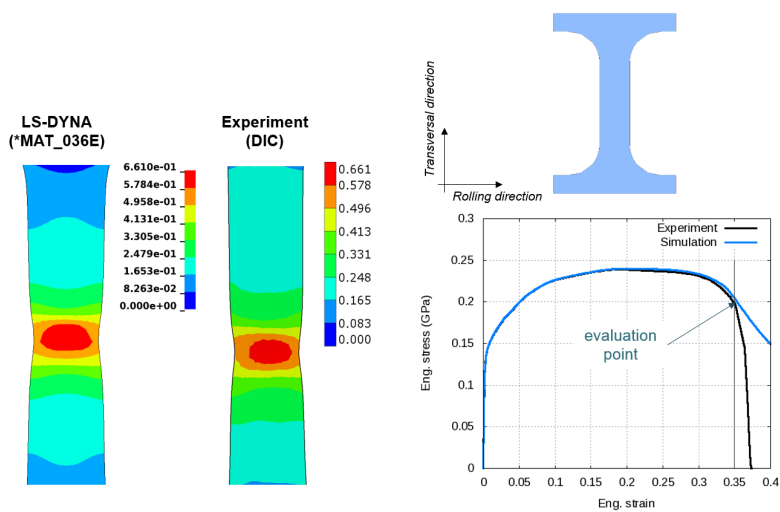


Fig.11: Comparison between experiment and simulation for the 90° direction

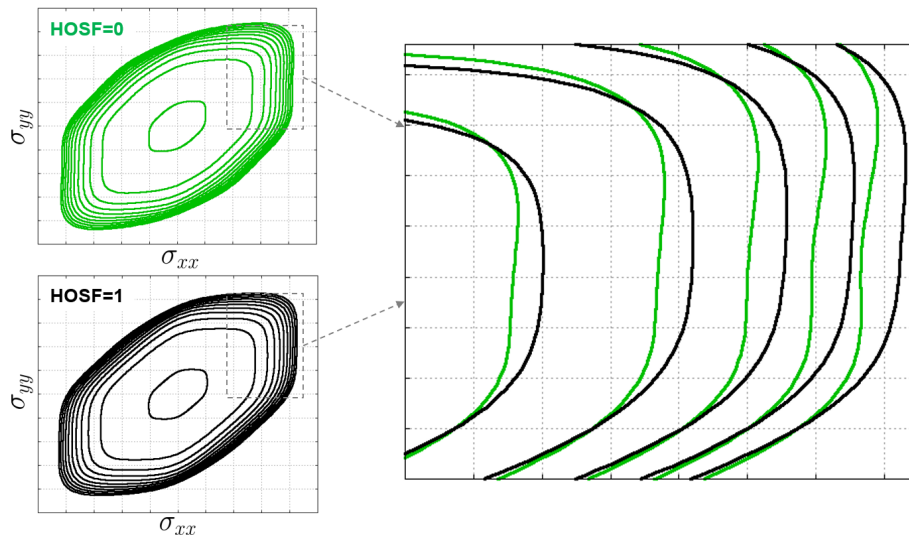


Fig.12: Comparison between the yield loci with HOSF=0 and HOSF=1 for the aluminum sheet

#### 4 Summary

In this paper, we presented a new orthotropic plasticity model. The model is implemented in LS-DYNA version R11 (or later) under \*MAT\_036E and can be activated whenever the option HOSF=1 is set. The novelty is the fact that the R values have no influence on the yield function. Instead, hardening curves for the different material orientations are used in order to accurately predict the onset of plastic straining. The R values are employed in the flow rule in order to describe the amount of plastic strain in the different material directions. The simulation of tensile tests in different directions for an aluminum sheet have shown that the model can accurately reproduce the local strain field observed in physical tensile tests as well as the global behavior through the engineering stress strain curves.

#### 5 Acknowledgements

The authors would like to thank Dr. David Koch, Dr. Martin Helbig and Christian Ilg for performing the experiments at the laboratories of DYNAmore in Stuttgart, Germany, and for providing the DIC data used in the comparison with the simulation results. Their help and support are greatly acknowledged.

#### 6 Literature

- [1] Barlat, F., Lian, J.: "Plastic behavior and stretchability of sheet metals. Part I: A yield function for orthotropic sheets under plane stress conditions", Int. J. Plasticity 5, 1989, 51-66.
- [2] LTSC: "LS-DYNA Keyword User's Manual – Volume II: Material Models", Livermore, 2019.
- [3] Lankford, W.I., Snyder, S.C., Bauscher, J.A.: "New criteria for predicting the press performance of deep-drawing sheets", Trans. ASM. 42, 1950, 1196-1232.
- [4] Hosford, W.F.: "A generalised isotropic yield criterion", J. Appl. Mech. 39, 1972, 607-609.
- [5] Koch, D., Helbig, M., Ilg, C.: "Experimental characterization of an aluminum sheet", Internal Report, 2017.